A New Archive of Apollo's Lunar Seismic Data

Ceri Nunn,[1,2], and Yosio Nakamura,[3], and Sharon Kedar,[1], and Mark Panning,[1]

Corresponding author: Ceri Nunn, Jet Propulsion Laboratory - California, Institute of Technology, Pasadena, U.S.A. (ceri.nunn@jpl.nasa.gov)

[1]Jet Propulsion Laboratory - California Institute of Technology, Pasadena, U.S.A.

[2] Ludwig-Maximilians-Universität, München, Deutschland

[3]Institute for Geophysics, John A. and Katherine G. Jackson School of Geosciences, University of Texas at Austin, Austin, Texas, U.S.A.

Abstract.

As a part of the Apollo lunar missions, the Apollo astronauts deployed seismic experiments on the nearside of the Moon between 1969 and 1972. Five stations collected passive seismic data. Apollo 11 operated for around twenty days and 12, 14, 15, 16 operated nearly continuously from their installation until 1977. Seismic data were collected and digitized on the Moon and telemetered to Earth. The data were recorded on digital magnetic tapes, with timestamps representing the signal reception time on Earth. The taped data have been widely used for many applications and have been previously shared in various formats. The data have slightly varying sampling rates, mainly due to the sensitivity of the data sampler to the significant temperature variations on the Moon's surface. Additionally, there were digital errors in the timestamps. Previously shared versions of the Apollo data were affected by these problems. We re-imported the passive data to SEED (Standard for the Exchange of Earthquake Data) format, and make these data available via IRIS (Incorporated Research Institutions for Seismology) and the PDS (Planetary Data System). We cleaned the timestamp series to reduce incorrectly recorded timestamps. The archive includes five tracks: three components of the mid-period seismometers, one short-period component and a time track which contains the timestamps. The seismic data are provided unprocessed in their raw format, and we provide instrument response files. We hope that the new archive will make it easier for a new generation of seismologists to use these data to learn more about the structure of the Moon.

1. Introduction

As a part of the Apollo lunar missions, the Apollo astronauts deployed seismic experiments on the nearside of the Moon between 1969 and 1972. Five stations collected passive seismic data (Fig. 1). Apollo 11 operated for around twenty days and 12, 14, 15, 16 operated nearly continuously from their installation until 1977, forming a lunar network. Fig. 2 shows data availability from the passive seismic experiments. The Passive Seismic Experiment was part of the Apollo Lunar Surface Experiment Package (ALSEP). The principal investigator was Gary Latham, initially of Colombia University and later of the University of Texas. The team comprised of a large group of scientists from many institutions, including the University of Texas, Massachusetts Institute of Technology and the University of Hawaii [*Latham et al.*, 1969, 1970].

The analysis of the seismic data from the Moon yielded many surprises. Fig. 3 shows the different types of lunar event. Deep moonquakes, located to depths of 700–1200 km [*Nakamura et al.*, 1982; *Nakamura*, 2005], were probably the most surprising. Peaks in deep moonquake activity had a periodicity of 27 days. Consequently, researchers associated the quakes with tides acting on the Moon [*Lammlein et al.*, 1974; *Lammlein*, 1977; *Nakamura*, 2005].

Shallow moonquakes, with possible depths between 50–220 km [*Khan et al.*, 2000] and estimated equivalent body-wave magnitude of 3.6–5.8 [*Oberst*, 1987] were also surprising. They may have a tectonic origin since they are similar to intraplate quakes on Earth [*Nakamura*, 1980]. Fig. 3 also shows examples of meteoroid strikes and artificial impacts.

The characteristics of the signals were also surprising when compared with terrestrial seismograms. Events of all types show long slow rise times and very slow decay of energy. The energy is strongly scattered, consistent with a highly fractured environment, especially near the surface. Duration of events can be as long as three hours, which requires very low attenuation compared to Earth. In total, [*Nakamura*, 1992] cataloged over 12000 events recorded on the mid-period seismometers.

Although seismic phases associated with the lunar core are challenging to see, recent work using stacked traces indicated a small lunar core (∼330–420 km in radius, *Weber et al.* [2011]; *Garcia et al.* [2011]). Recent observations from the GRAIL gravity mission suggested average crustal porosity of 12%, which is higher than previous estimates, and consistent with a highly fractured crust [*Wieczorek et al.*, 2013]. Using the higher estimates of porosities, the team modeled the average crustal thickness to be 34–43 km.

Various space agencies are planning future lunar missions, including seismic missions. NASA's Farside Seismic Suite, which is due to fly in the mid-2020s, will visit Schr´odinger Crater. One of its mission objectives is to determine whether the Moon's farside is as seismically active as the nearside [*Panning et al.*, 2021]. The Lunar Geophysical Network, which will contain a network of seismometers and geophysical instruments spread around the Moon at up to four landing sites, will be proposed to NASA's New Frontiers 5 [*Neal et al.*, 2020]. Existing observations from the Apollo network will continue to be useful to compare with these future missions.

Data from all of the experiments in the Apollo Lunar Surface Experiment Package were collected on magnetic tapes. As the tapes deteriorate, the data are in great danger of being lost. As a part of NASA's Planetary Data Archiving, Restoration, and Tools project (PDART), an effort is being made to recover and archive as much of the data and metadata as possible [*Nagihara et al.*, 2017].

We provide a new version of the passive data in SEED format (Standard for the Exchange of Earthquake Data). There are two major obstacles to formatting the data in a modern format. The first problem is that the sampling interval is temperature-dependent and consequently varies with the time of lunar day. The second problem is that the timestamp records when the signal arrived on Earth rather than when the instrument took the measurement. This problem introduces a delay and adds additional time variation related to the rotation of the Earth, the libration of the Moon, and the Moon-Earth distance. Modern formats, such as SEED, require constant sampling rates. We solve this problem with a compromise. We give the data a constant sampling interval (the mid-period and short-period data have nominal sampling intervals of 0.1509434 s and 0.0188679 s, respectively). However, we retain a separate track that contains the timestamps. We see a slight positive or negative drift of a few seconds after 24 hours, which is different for different stations. The time track contains information about the actual sampling interval at any given time. We provide the data in the original raw format so that users can control the data processing that they apply.

We begin this paper with a description of the Apollo seismometers. Next, we describe the steps to extract the data. We follow with a description of the data in the new archive. We end with a summary of how to access the archive.

2. Description of the Apollo Seismometers

Our data archive covers the passive experiments, which included mid-period and short-period instruments. Here we provide a brief description of the seismometers (see *Nunn* *et al.* [2020] for more information). The mid-period seismometer contained three matched sensors aligned orthogonally to measure one vertical (MHZ) and two horizontal components (MH1, MH2) of surface motion. The seismometer made measurements proportional to displacement, unlike most modern seismometers covering these frequencies, which make measurements proportional to velocity. The nominal sampling interval was 0.1509434 s.

The instrument could operate in one of two modes (Fig. 4): flat-response or peaked-response mode. In the flat-response mode, the seismometers had natural periods of 15 s and could detect ground motions as small as 0.3 nm over the frequency range from 0.1 Hz to 1 Hz, *Latham et al.* [1973]). In flat-response mode, a positive feedback circuit extended the bandwidth of the instrument. In peaked-response mode, the signal bypassed the feedback filter, and the transfer function was sharply peaked at 2.2 s. The seismometers acted as underdamped pendulums [*Latham et al.*, 1973]. Maximum sensitivity in the peaked mode was 5.6 times greater than the flat mode, but low-frequency sensitivity was reduced [*Latham et al.*, 1973]. S14 was unstable in the flat-response mode most of the time since the feedback parameters were specified incorrectly. Fig. 2 shows the times when the seismometer was operating in peaked or flat mode.

The short-period sensor was a vertical sensor with a standard coil-magnet velocity transducer. It had a displacement response peaked at approximately 8 Hz (Fig. 4), and the nominal sampling interval was 0.0188679 s.

3. Importing to SEED format

In this section, we describe how the data were recorded, and the steps involved in processing it for SEED format. The data were stored in a binary format on magnetic tapes. Copies of the original tapes are available from the Japanese Space Agency [*JAXA*, 2012]. The data were received at a ground station on Earth. The ground stations were spaced around the Earth, and at least three stations would operate over 24 hours, to maintain a good line of sight to the Moon. Often, during the transition from one station to another, there was a brief overlap where two stations were recording simultaneously, although gaps were also common.

3.1. Step 1 - Extracting the data from the tape copies

We extracted the data from the binary using the data schema described in *Nakamura* [1992]. The data sampler on the Moon recorded the data in blocks (physical records) of 90 frames each. Within each frame, the data were arranged into 64 10-bit ALSEP words, evenly spaced in time. Each component of the mid-period seismometers (MH1, MH2, and MHZ) recorded four samples per frame. SHZ used the even words within the block except for words 2, 46, 56. Additionally, S15 contained an error which meant that word 24 was also missing on S15. Thus, the SHZ timing is evenly spaced, but with 3 or 4 missing data samples per frame. The sampling interval is 16/106 s or 0.1509434 s for the mid-period instruments and 2/106 s or 0.0188679 s for the short-period instruments.

The data sampler transmitted each data frame to Earth in real-time. The computer recorded the timestamps at the head of each frame when the transmission arrived on Earth.

3.2. Step 2 - Error Checking

We checked the extracted data for errors, beginning with checking the Barker code. The transmission contained a Barker code, which is a code with a series of zeros and ones in a preset pattern. An intact Barker code indicates that the receiver read the transmission correctly. The traces show that when the Barker code was incorrect, the corresponding data samples were meaningless. We rejected all data with damaged Barker codes (approximately 0.3% of all the available data). We also examined the traces to determine whether we could extract data from a damaged trace (for example, by shifting the zeros and ones to find a match to the Barker code). However, this did not seem possible. Transmission errors usually occurred in blocks. The blocks could begin or end at any point in the frame and affect all data between the endpoints. Damaged traces could run consecutively for minutes or hours or be more sporadic. Our despiking algorithm (see Step 3, below) includes code to deal with this problem of frames that are partially damaged (including those which occur before data which we removed due to the damaged Barker code).

The data were recorded alongside a frame number, which ranges from 0 to 89. The frame was recorded by the sampler and transmitted with the data. This number helps correctly determine when traces overlap (due to recording at two ground stations). When the data were not being received correctly, they were often re-transmitted, and these re-transmissions were recorded on the tapes. A repeated frame number with timestamps close to each other indicates re-transmission. We found cases where the sampler reset the frame number to zero before finishing the previous physical record, although these cases are rare.

When two ground stations received data simultaneously, the timestamps did not match exactly. We expect slight timestamp differences because the lines of sight from the seismic station on the Moon to the two different ground stations were not the same. These differences are in addition to errors caused by unsynchronized reference clocks at the stations or difficulties reading the clocks. We take advantage of the fact that the data are transmitted in real-time to test for errors in the transmission. For example, the timestamp is probably incorrect if it suddenly jumps forward or backward in time. The binary data could be damaged either during transmission or later, as the tapes deteriorated. Therefore, flipped bits could damage the timestamp, the frame number, the station code, the ground station, or the sensor data.

Although the data did not have constant sampling intervals, most sample intervals fell within a narrow range. A nominal frame is 0.6038 s. Nearly all sample intervals are either 0.603 s or 0.604 s (we expect this because the precision of the timestamp is only 0.001 s). We make the following corrections to the data. We amended single frame numbers which were out of sequence but had the correct timestamps. We also amended single timestamps, which were out of series but had the correct frame numbers. Next, we determined sections of traces with 'good' records - those which had a single sampling interval (> 0.6009 s and < 0.607 s) and a single gap between frames. We found if these traces are consecutive. We tried to amend the timestamps by using the last record of a consecutive block and the first record of the next consecutive block. Where there were transmission gaps, we inserted the correct number of empty samples between frames (using a combination of time and the frame gap). We ignored small errors in the sampling interval at this stage. Finally, we dropped any remaining records which were in sections that do not contain at least 180 consecutive good records.

To reduce timing errors, we kept only sections of traces with at least 180 consecutive frames ($\sim$109 s). These sections may contain gaps in the sampling, but we require interpolated timestamps and frame numbers that fit the correct number of frames and the sampling interval. This precaution prevents random timing errors. However, if the local clock were incorrect, this method would be unable to prevent the error. Unfortunately, our approach could exclude potentially valid data when the sampler was running particularly fast or slow.

The time the signal arrived on Earth was usually determined by a standard time signal received at the ground station. However, when the computer could not read the standard signal, it would generate a timestamp [*Nakamura*, 2011; *Knapmeyer-Endrun and Hammer*, 2015, supplement]. The 'software clock' could lead to offsets of more than one minute, in comparison with the standard time [*Nakamura*, 2011]. We check for suspected use of the software clock, and where possible, we interpolate the timestamp as a continuous trace. From 1973, the team added a flag to the tapes to indicate the use of the software clock. When the flag was set, we corrected the timestamps by interpolation, resulting in no offsets.

From March 1976 until the end of the mission, the University of Texas Galveston Geophysics Laboratory collected data on work tapes, including all the stations (except S11). We noticed some specific errors with these tapes. For example, we found a section of the traces copied from S12 to S14 within the tape from approximately 22:00 to 22:30 on 1976-12-05. We tried to search for these errors and exclude the data. When viewing the copied traces, we find a section of S14 that jumps from being centered around 498 digital units to one centered around 516 digital units with a much noisier trace. Sudden jumps in the centerline, or sudden changes in the noise profile, are warning signs, and users should be careful using traces where they notice these errors.

3.3. Step 3 - Making the SEED files

In the final step, we make SEED files from the cleaned data. Where possible, we try to construct traces with continuous sampling. Although these traces may contain small gaps in the data sampling, the timing trace is continuous. As explained in the previous section, we use the frame numbers combined with the timestamps to determine where these gaps should be.

When constructing the SEED files, there is a sample time, and a timestamp time. The sample time is based on the nominal sampling interval and the number of samples. The timestamp is based on the time the sample was received on Earth. To estimate the start time of any trace, we estimate the number of samples since midnight using the actual sampling interval. We can then calculate the sample time using nominal sampling interval. At midnight, these times are the same, but they diverge during the day.

To construct the continuous trace, we check for an overlap and try to match the frame number. If we can match the frame number, we set the start time of the new trace at this time. If we cannot match the frame number in the overlapped trace, this is an error with either the new or old trace. We start the new trace at the new time and record an error in the log. If there is no overlap, we try to fit a gap with an exact number of frames between the end of the previous trace and the following trace. If matched, we start the new trace at the correct time to take account of the gaps. If we cannot fit an exact gap, we use the current time (based on an estimation of the currently sampling interval) and estimate the start time of the sample. We record the potential error in the log.

The output SEED file is a single file from a few milliseconds after midnight until the following night. Note that the trace will not finish at exactly midnight and may go slightly over into the next day because we reconstruct a continuous trace with a nominal sampling rate that does not precisely match the actual sampling rate (which will also vary during the day). When traces overlap, if one trace has missing samples, these are filled by samples from the other trace.

We run a despiking algorithm on the trace (Fig. 5). We designed the algorithm to remove single digital spikes only. These occur when a single data point is incorrectly recorded (probably caused by a flipped bit during transmission). We remove these at this stage because they are relatively easy to remove and are not related to the function of the seismometer. Fig. 6 shows the process of data cleaning. The top trace shows the original data. The middle trace shows data imported, excluding the data damaged in transmission (we excluded data if the Barker code was incorrect). The bottom trace has also been despiked.

4. Description of the Archived Data

This section describes how to understand the data. We provide five tracks of data (Fig. 7), three components on the mid-period seismometers (MH1, MH2, and MHZ), the short-period sensor (SHZ), and a timing trace, ATT. Each data track is in raw format. We name the mid-period channels as MH1, MH2, MHZ to be consistent with the IRIS naming conventions. The 'M' reflects mid-period data and a sampling rate between 1 and 10 Hz. The 'H' is for a high gain seismometer. Finally, since the horizontal channels do not always point north or east, we use 1 and 2 to indicate the channel orientations. The correct orientations are in the metadata for the SEED files. Earlier papers referred to these channels as long-period. MH1, MH2, and MHZ directly correspond to LPX, LPY, and LPZ from earlier papers. The mid-period seismometers ran in either flat or peaked mode. We split the files into locations '00' for the peaked mode and '01' for the flat mode. The location field is blank for SHZ and the timing trace ATT.

As described above, there are missing samples for the SHZ traces. We substitute a value of minus one for each of these missing values on the traces. We also do this for missing samples on the mid-period traces. The traditional approach to missing samples is to mask the traces in the SEED file. However, we found that the missing samples were so frequent that the data files were significantly larger and there were performance issues when using this traditional approach. Users should read in the traces, and replace the minus one values with masks or interpolate the data. There is a code snippet on our GitHub repository (github.com/cerinunn/pdart) to do this. Users may also find it helpful to remove glitches before beginning their analysis, since our despiking algorithm removes only single digital spikes.

The ATT tracks contain the timestamp, measured in seconds from 01/01/1970 (timestamps from 1969 are negative). The time can be recovered easily with ObsPy [*Beyreuther et al.*, 2010], using the class UTCDateTime (e.g. the command `UTCDateTime(-14182916.0)` will recover `1969-07-20T20:18:04.000000Z`). Note that the original data recorded on the tapes used a different convention for the timestamps. The sampling rate for the timing trace is 0.6037735849 s because the timing was recorded once per frame.

The data were recorded with digital units (DU), with values from 0 to 1023. The values lay somewhere in the middle of the range when the seismometer was at rest, although the rest position varies with the time of lunar day. One digital unit corresponded to ~0.08 nm of ground displacement in peaked-response mode and ~0.3 nm in flat-response mode at

0.45 Hz. Users can transform the data into displacement, velocity, or acceleration with the provided SEED metadata files.

The samples for each of the mid-period sensors were not taken simultaneously, which has implications when comparing signals on the three components. The first MH1 sample (ALSEP word 9) was sampled 10/1060*8=0.075 s after the head of the frame. MH2 and MHZ were sampled 0.094 and 0.113 s after the head of the frame. SHZ is sampled at every even position and so begins at 10/1060*8=0.015 s after the head of the frame (note that the first position was blank but is included in the timing). We provide the MH1, MH2, MHZ and SHZ traces with a time-shift of 0.075, 0.094, 0.113, and 0.015 s relative to the ATT and AFR traces.

We constructed the SEED files with the nominal sampling rate. Therefore, there can be a positive or negative time shift of up to a few seconds after twenty-four hours, as shown in Fig. 8. In some situations, data users may find removing the drift helpful by using the information provided on the timing trace ATT.

There is a 1.2–1.4 s delay time when transmitting from the Moon to Earth, which we do not correct for. Additionally, we do not correct for the apparent variations in sampling rate which are caused by changes in the orbital parameters of the Moon-Earth system, such as by the rotation of the Earth, the libration of the Moon or changes in Moon-Earth distance.

The sampling interval was strongly dependent on whether it was lunar day or night (Fig. 9a). Sampling was reasonably constant during lunar night, but strong variations occurred during the day, especially at sunrise and sunset. This variation was probably caused by strong temperature fluctuations on the lunar surface. This was because the oscillator that controlled the sampling was not temperature compensated. In addition there were short-term fluctuations in the sampling interval. The rotation of the Earth also had a small effect on the apparent sampling interval (Fig. 9b).

There are therefore many errors associated with the timing: variability of the sampling on the Moon, reception errors, recording errors, the distance from the source of the standard time signal to the ground station, and variation introduced by the rotation of the Earth, the libration of the Moon and the distance from the Moon to the Earth. Only the first of these errors affected the actual sampling rate. The others only affect the apparent sampling rate. Therefore, the recorded sampling interval is only a guide to the actual sampling interval.

The team were able to send commands to the seismometers. The commands included options to change the seismometer gain, to send calibration pulses, and to change the mode of the mid-period seismometer from flat to peaked or vice versa. The timing of these commands is included in our GitHub site (github.com/cerinunn/pdart/) along with an example calibration pulse.

We provide the nominal instrument responses in the SEED metadata files. *Horvath* [1979] evaluated the differences between the nominal transfer functions provided by the engineers (and provided within the response files) and the actual transfer functions. The actual transfer functions had some differences between stations and over the lifetime of the instruments. The team sent calibration pulses to the seismometers. A step of current equivalent to a known step of ground acceleration was applied to the coil for each of the seismometer components [*Latham et al.*, 1973]. Additionally, the engineers controlled the gain from Earth, and were able to cycle through the options (from maximum gain, -10 dB,

-20 dB, -30 dB and back to maximum). The timing of the gain commands is known, and provided on our github site (github.com/cerinunn/pdart/), but the resulting gain can only be found by checking the seismograms. In general, the seismometers operated at maximum gain.

5. Data Archive

We are currently archiving the data at IRIS, where it will be possible to download it using network code XA. We are also archiving the data on the Geosciences Node at the Planetary Data System. [Note to reviewers: We have uploaded test uploads to both IRIS and the PDS. We think it is likely that the IRIS archive will be ready prior to publication. The PDS requires a review process which may take 3-4 months, so is also reasonably likely to be ready prior to publication.] Fig. 10 shows the percentage of data recovered and placed into the archive.

6. Data and Resources

Our GitHub repository (github.com/cerinunn/pdart/tree/master/Electronic_Supplement) includes the following additional information: the locations of the seismic stations; the operational status of the instruments; the timing of commands sent to the instruments; the times when the mid-period seismometers were operating in flat mode; the codes for the ground stations receiving the signals; and example calibration pulses.

The data described within this paper is archived at IRIS with the following DOI: https://doi.org/10.7914/SN/XA_1969. [Note to reviewers: We have uploaded test data to IRIS. IRIS have checked the data. The data will be released to coincide with the publication of this companion paper.] The data are also archived at the Geosciences Node of the Planetary Data System: https://pds-geosciences.wustl.edu/. [Note to reviewers: We have uploaded test data to the PDS. The PDS will send the data out for an independent review.] If use is made of this work, authors should cite *Latham et al.* [1970], *Yamada et al.* [2012], as well as this paper.

We used ObsPy extensively during this project [*Beyreuther et al.*, 2010]. Figures have been produced with the Python tool Matplotlib [*Hunter*, 2007]. Fig. 1 was produced with Cartopy [*Met Office*, 2010] using topographic data from [*Araki et al.*, 2009].

Acknowledgments. This work was finalized with a grant from the National Aeronautics and Space Administration's Planetary Data Archiving, Restoration, and Tools (PDART), proposal number 19-PDART19_2-0052, task number 811073.02.37.01.99 and also support from strategic funds from the Jet Propulsion Laboratory, California Institute of Technology, under a contract with the National Aeronautics and Space Administration. The work was initially funded with the European Union's Horizon 2020 research and innovation program under the Marie Sklodowska-Curie grant agreement No. 659773. This work benefited from discussions at the workshop 'An International Reference for Seismological Data Sets and Internal Structure Models of the Moon' supported by the International Space Science Institute, Bern, Switzerland.

References

Araki, H., S. Tazawa, H. Noda, Y. Ishihara, S. Goossens, S. Sasaki, N. Kawano, I. Kamiya, H. Otake, J. Oberst, and C. Shum (2009), Lunar Global Shape and Polar Topography derived from Kaguya-LALT Laser Altimetry, *Science*, *323*(5916), 897–900, doi: 10.1126/science.1164146.

Bates, J. R., W. W. Lauderdale, and H. Kernaghan (1979), ALSEP Termination Report.

Beyreuther, M., R. Barsch, L. Krischer, T. Megies, Y. Behr, and J. Wassermann (2010), ObsPy: A Python Toolbox for Seismology, *Seismol. Res. Lett.*, *81*(3), 530–533, doi: 10.1785/gssrl.81.3.530.

Garcia, R. F., J. Gagnepain-Beyneix, S. Chevrot, and P. Lognonné (2011), Very preliminary reference Moon model, *Phys. Earth Planet. Int.*, *188*(1–2), 96–113, doi: 10.1016/j.pepi.2011.06.015.

Horvath, P. (1979), Analysis of Lunar Seismic Signals: Determination of Instrumental Parameters and Seismic Velocity Distributions., Ph.D. thesis, University of Texas at Dallas.

Hunter, J. D. (2007), Matplotlib: A 2D Graphics Environment, *Comput. Sci. Eng.*, *9*(3), 90–95, doi:10.1109/MCSE.2007.55.

JAXA (2012), Original Exabyte Format Data Files, https://www.darts.isas.jaxa.jp/planet/seismology/apollo/GET_Exabyte.html.

Khan, A., K. Mosegaard, and K. L. Rasmussen (2000), A new seismic velocity model for the Moon from a Monte Carlo inversion of the Apollo lunar seismic data, *Geophys. Res. Lett.*, *27*(11), 1591–1594, doi:10.1029/1999GL008452.

Knapmeyer-Endrun, B., and C. Hammer (2015), Identification of new events in Apollo 16 lunar seismic data by Hidden Markov Model-based event detection and classification, *J. Geophys. Res. Planets*, *120*(10), 1620–1645, doi:10.1002/2015JE004862.

Lammlein, D. R. (1977), Lunar seismicity and tectonics, *Phys. Earth Planet. Int.*, *14*(3), 224–273, doi:10.1016/0031-9201(77)90175-3.

Lammlein, D. R., G. V. Latham, J. Dorman, Y. Nakamura, and M. Ewing (1974), Lunar seismicity, structure, and tectonics, *Rev. Geophys.*, *12*(1), 1–21, doi: 10.1029/RG012i001p00001.

Latham, G., M. Ewing, F. Press, and G. Sutton (1969), The Apollo Passive Seismic Experiment, *Science*, *165*(3890), 241–250.

Latham, G., M. Ewing, J. Dorman, Y. Nakamura, F. Press, N. Toksőz, G. Sutton, F. Duennebier, and D. Lammlein (1973), Lunar Structure and Dynamics - Results from the Apollo Passive Seismic Experiment, *The Moon*, *7*(3-4), 396–421, doi: 10.1007/BF00564643.

Latham, G. V., M. Ewing, F. Press, G. Sutton, J. Dorman, Y. Nakamura, N. Toksoz, R. Wiggins, J. Derr, and F. Duennebier (1970), Passive Seismic Experiment, *Science*, *167*(3918), 455–457, doi:10.1126/science.167.3918.455.

Met Office (2010), Cartopy: A cartographic python library with a matplotlib interface, http://scitools.org.uk/cartopy, last accessed 2017-09-11.

Nagihara, S., Y. Nakamura, D. R. Williams, P. T. Taylor, S. A. McLaughlin, H. K. Hills, W. S. Kiefer, R. C. Weber, J.-L. Dimech, D. Phillips, C. Nunn, and G. K. Schmidt (2017), Recent achievement by the SSERVI ALSEP data recovery focus group, *2017 Annu. Meet. Lunar Explor. Anal. Group LEAG*, abstract #5017.

Nakamura, Y. (1980), Shallow moonquakes - How they compare with earthquakes, *Proc. 11th Lunar Planet. Sci. Conf.*, pp. 1847–1853.

Nakamura, Y. (1992), Catalog of lunar seismic data from Apollo passive seismic experiment on 8-mm video cassette (Exabyte) tapes, *UTIG Tech. Rep. No. 118, Institute for Geophysics, The University of Texas at Austin.*

Nakamura, Y. (2005), Farside deep moonquakes and deep interior of the Moon, *J. Geophys. Res.*, *110*(E01001), doi:10.1029/2004JE002332.

Nakamura, Y. (2011), Timing problem with the Lunar Module impact data as recorded by the LSPE and corrected near-surface structure at the Apollo 17 landing site, *J. Geophys. Res.*, *116*(E12005), doi:10.1029/2011JE003972.

Nakamura, Y., G. V. Latham, and H. J. Dorman (1982), Apollo Lunar Seismic Experiment – Final summary, *J. Geophys. Res.*, *87*(S01), A117–A123, doi:10.1029/JB087iS01p0A117.

Neal, C., R. C. Weber, M. Amato, J., A. Seas, S. Team, and E. Team (2020), The Lunar Geophysical Network (Planetary Missions Concept Studies Report), *Tech. Rep. Submitted in response to: NNH18ZDA001N-PMCS*.

Nunn, C., R. F. Garcia, Y. Nakamura, A. G. Marusiak, T. Kawamura, D. Sun, L. Margerin, R. Weber, M. Drilleau, M. A. Wieczorek, A. Khan, A. Rivoldini, P. Lognonné, and P. Zhu (2020), Lunar Seismology: A Data and Instrumentation Review, *Space Science Reviews*, *216*(5), 89, doi:10.1007/s11214-020-00709-3.

Oberst, J. (1987), Unusually high stress drops associated with shallow moonquakes, *J. Geophys. Res.*, *92*(B2), 1397–1405, doi:10.1029/JB092iB02p01397.

Panning, M. P., S. Kedar, N. Bowles, S. Calcutt, J. Cutler, J. O. Elliott, R. F. Garcia, T. Kawamura, P. H. Lognonné, E. A. Miller, C. Nunn, W. T. Pike, G. Pont, S. De Raucourt, I. M. Standley, W. Walsh, R. C. Weber, and C. Yana (2021), Farside Seismic Suite (FSS): First seismic data from the farside of the Moon delivered by a commercial lander, in *AGU Fall Meeting 2021*.

Wagner, R. V., D. M. Nelson, J. B. Plescia, M. S. Robinson, E. J. Speyerer, and E. Mazarico (2017), Coordinates of anthropogenic features on the Moon, *Icarus*, *283*(Supplement C), 92–103, doi:10.1016/j.icarus.2016.05.011.

Weber, R. C., P.-Y. Lin, E. J. Garnero, Q. Williams, and P. Lognonné (2011), Seismic Detection of the Lunar Core, *Science*, *331*(6015), 309–312, doi:10.1126/science.1199375.

Wieczorek, M. A., G. A. Neumann, F. Nimmo, W. S. Kiefer, G. J. Taylor, H. J. Melosh, R. J. Phillips, S. C. Solomon, J. C. Andrews-Hanna, S. W. Asmar, A. S. Konopliv, F. G. Lemoine, D. E. Smith, M. M. Watkins, J. G. Williams, and M. T. Zuber (2013), The Crust of the Moon as Seen by GRAIL, *Science*, *339*(6120), 671–675, doi:10.1126/science.1231530.

Yamada, R., Y. Yamamoto, Y. Nakamura, and J. Kuwamura (2012), A New Retrieval System of Apollo Lunar Seismic Data with Data Correction, *43rd Lunar Planet. Sci. Conf.*, abstract #1712.

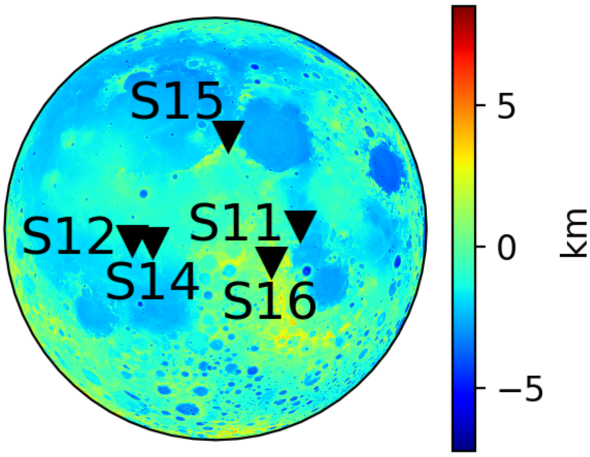

Figure 1. Locations of the Seismic Stations. The plot shows the locations of the stations included in the archive. The background shows lunar topography from *Araki et al.* [2009].

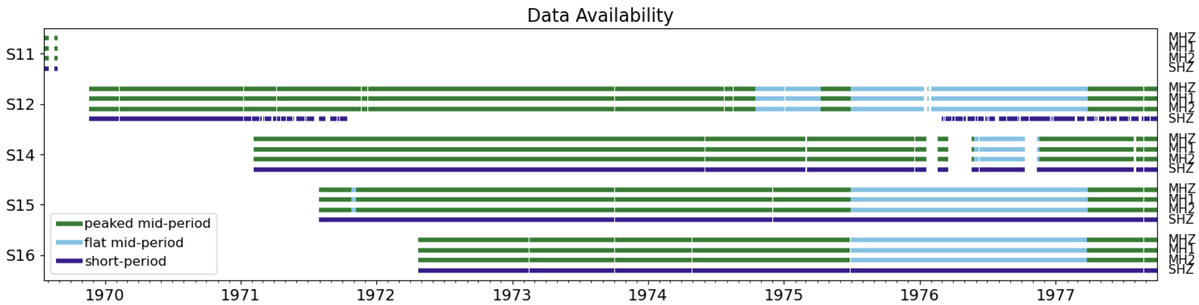

Figure 2. Seismic Data Availability. The experiments included three-component mid-period instruments (MHZ, MH1, and MH2) which operated in either peaked mode (green lines) or flat mode (light-blue lines) and short-period instruments (SHZ, dark-blue lines).

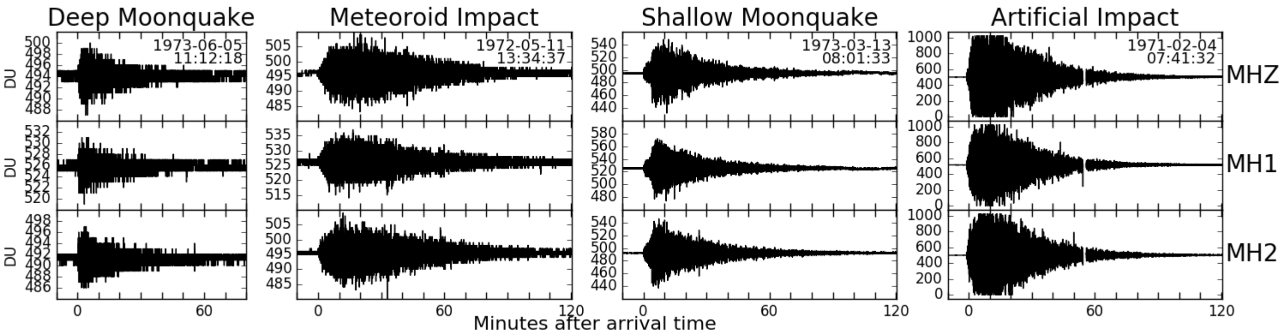

Figure 3. Examples of a Deep Moonquake, a Meteoroid Impact, a Shallow Moonquake and an Artificial Impact Event. The events were recorded on seismic station S12 on three components (MHZ, MH1 and MH2). The timing for each event is in minutes and relative to arrival time. The y-axis scale is in digital units (DU), and the scale is different for each of the events. The amplitude of the impact signal exceeded the range of the instrument.

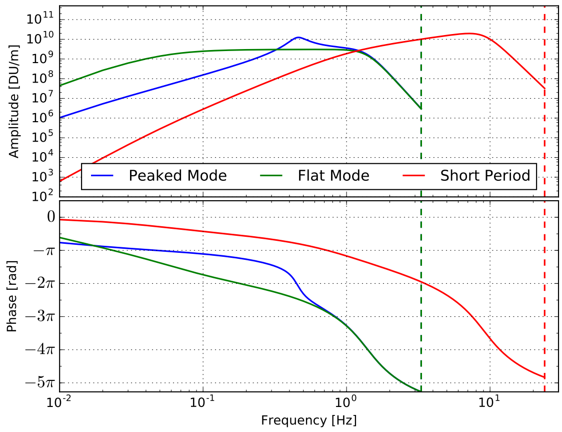

Figure 4. Transfer Functions. Displacement amplitude (top) and phase (bottom) transfer functions for the flat and peaked modes of the mid-period seismometer and the short-period (SP) seismometer. The plots show the nominal responses up to the Nyquist frequency (dashed lines). The units of amplitude are Digital Units (DU) per meter. The phases show the counterclockwise angle from the positive real axis on the complex plane in radians. The transfer functions in velocity and acceleration are available in *Nunn et al.* [2020].

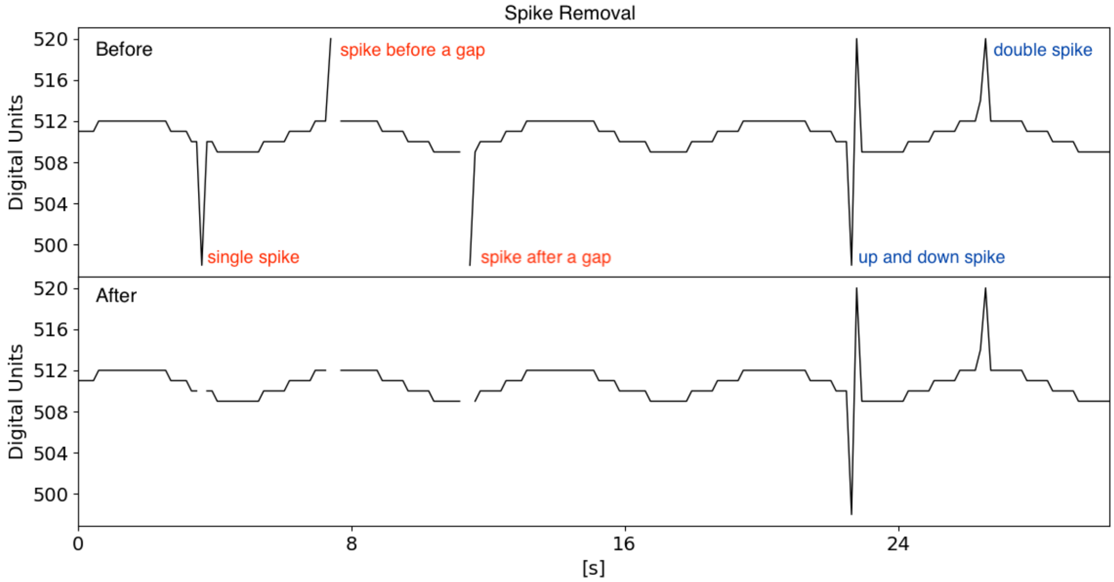

Figure 5. Digital Spike Removal. The top panel shows test data with added digital spikes, and the bottom panel shows the data after the spike removal process. The algorithm removes single spikes, spikes before a gap, and spikes after a gap. Up and down spikes and double spikes (which have two data points within the spikes) are not removed by the algorithm.

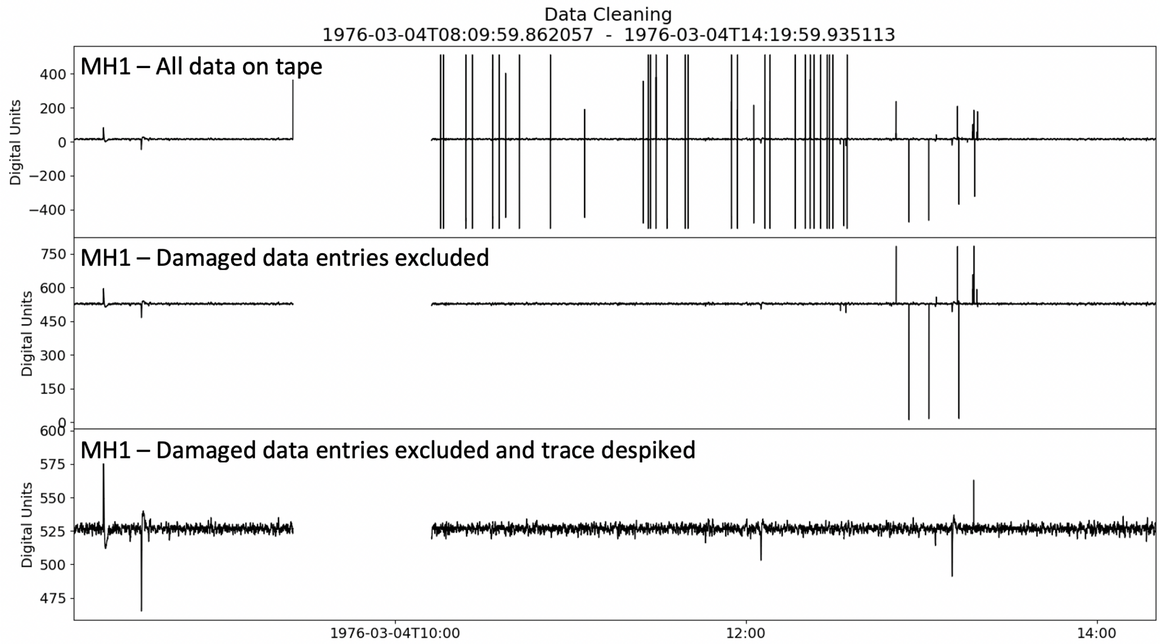

Figure 6. Data Cleaning. The top panel shows the original data imported from the tape. The middle panel shows the same data re-imported, including only the data with correct Barker codes (incorrect Barker codes indicate data frames that were not transmitted correctly). The bottom panel shows the data after we removed single digital spikes (Fig. 5 shows examples of these spikes).

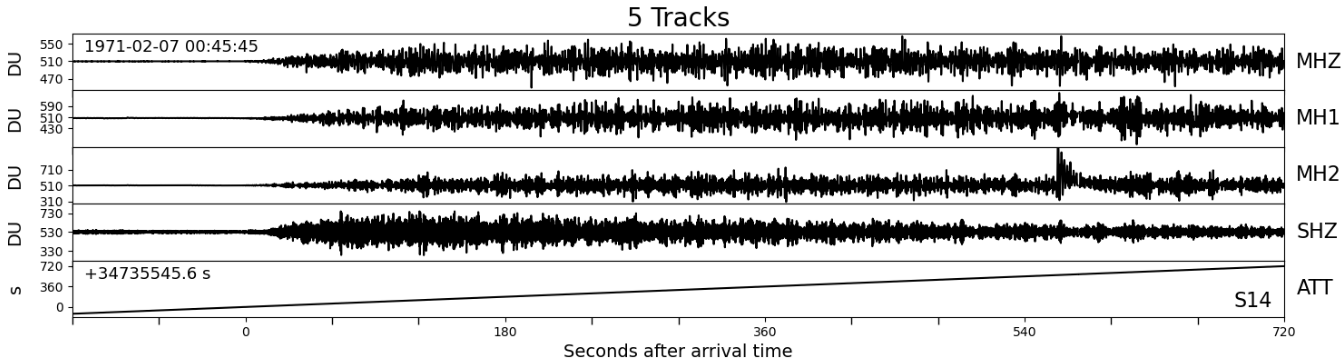

Figure 7. Data Tracks provided in the SEED Files. The top four traces show the data traces MHZ, MH1, MH2, and SHZ. The x-axis is seconds after the P arrival time, and the y-axis is in digital units (DU). The fifth trace ATT shows the timestamp (seconds since 1970-01-01) recorded at the ground station. The timing is in seconds relative to the arrival time (34735545.6 s after 1970-01-01).

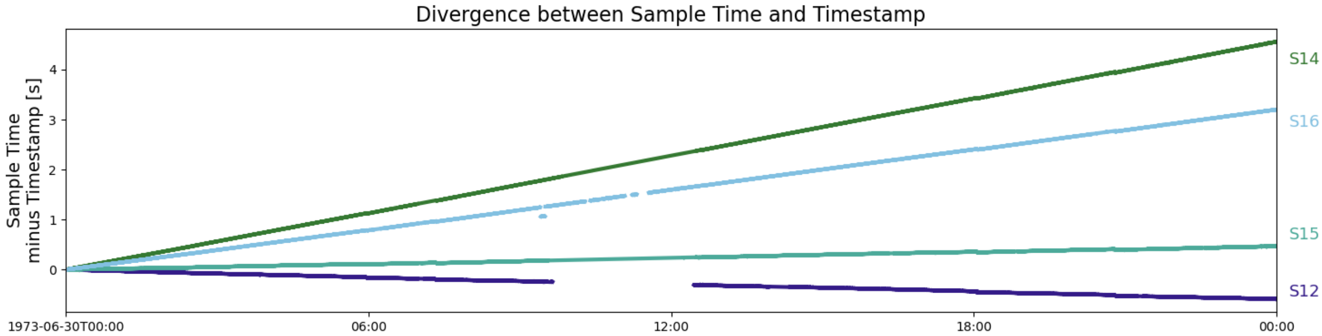

Figure 8. Divergence between Sample Time and Timestamp. Each of the data samplers controlling the sampling on the seismometers had a slightly different sampling rate that varied over time. As far as possible, the data are provided as continuous traces. Therefore, there is some divergence between the time estimates from the continuous sampling and the recorded timestamps. Data users should be aware of these differences and may need to correct for them. The divergence lines are curved. Additionally, the S12 trace shows a gap were data were not recovered due to timing issues and the S16 trace shows 9:25 to 9:30 where there is a problem with the timing. Where possible, sections of traces with timing issues should be avoided.

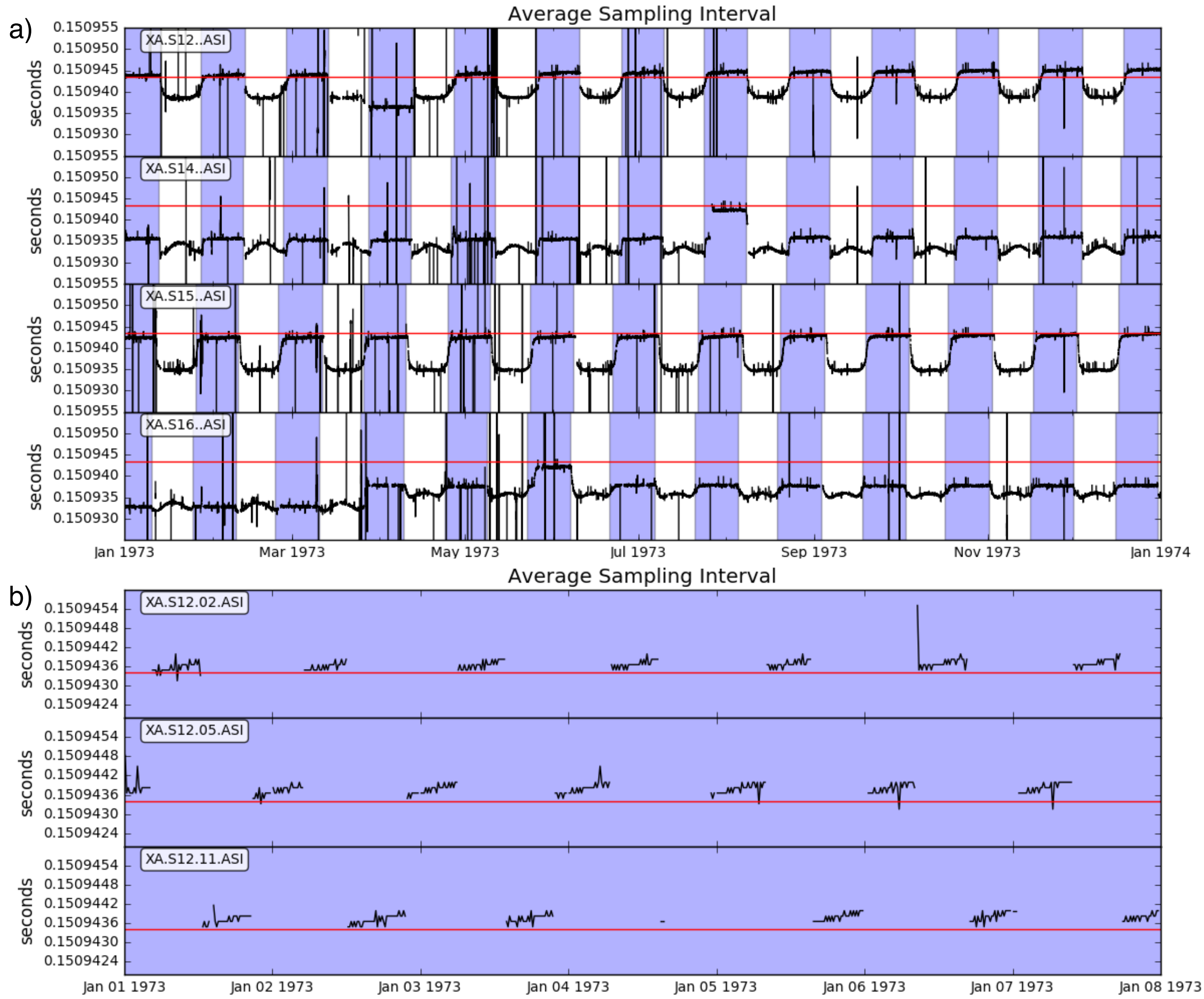

Figure 9. Variation in the Sampling Interval. a) The variability of the sampling interval for each of the stations during 1973. b) The variability of the sampling interval from 1–7 January 1973 for station S12 recorded at different ground stations (02, Ascension Island; 05, Guam; 11, Corpus Christi, Texas). The rotation of the Earth has a small affect on the apparent sampling rate (it does not affect the real sampling rate). The increase in the apparent sampling rate while a ground station is recording on (b) is due to the rotation of the Earth. The apparent sampling rate is lower when a new ground station starts recording. In both plots, we averaged the sampling over approximately 15 minutes. The plots show alternating periods of lunar night (purple) and lunar day (white). The red lines show the nominal sampling interval (0.1509434 s).

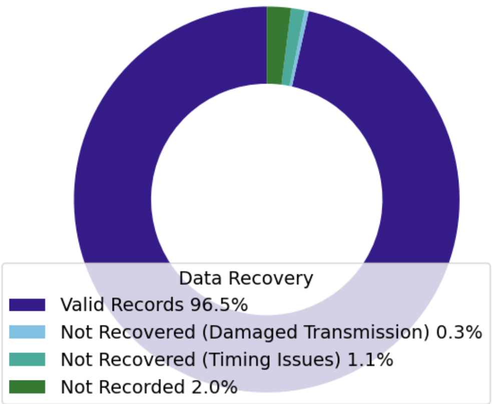

Figure 10. Data Recovery. For the duration of the mission at station S12, S14, S15 and S16, the percentage of valid records, records which were damaged during transmission, records which were not recovered by us due to timing issues, and records which were not recorded by the mission. Note that periods of time when the seismometers were transmitting data but not sending back valid seismic records are not excluded from the estimation of valid records.